International Journal of Minerals, Metallurgy and Materials
Volume 23, Number 8, August 2016, Page 934
DOI: 10.1007/s12613-016-1309-x

Microstructure studies of air-plasma-spray-deposited CoNiCrAlY coatings before and after thermal cyclic loading for high-temperature application

*Dipak Kumar*1), *K.N. Pandey*1), *and Dipak Kumar Das*2)

1) Mechanical Engineering Department, Motilal Nehru National Institute of Technology, Allahabad-211004, India
2) Defense Metallurgical Research Laboratory, Hyderabad-500058, India

(Received: 25 February 2016; revised: 12 April 2016; accepted: 13 April 2016)

Abstract: In the present study, bond-coats for thermal barrier coatings were deposited via air plasma spraying (APS) techniques onto Inconel 800 and Hastelloy C-276 alloy substrates. Scanning electron microscopy (SEM), transmission electron microscopy (TEM), X-ray diffraction (XRD), and atomic force microscopy (AFM) were used to investigate the phases and microstructure of the as-sprayed, APS-deposited CoNiCrAlY bond-coatings. The aim of this work was to study the suitability of the bond-coat materials for high temperature applications. Confirmation of nanoscale grains of the γ/γ'-phase was obtained by TEM, high-resolution TEM, and AFM. We concluded that these changes result from the plastic deformation of the bond-coat during the deposition, resulting in CoNiCrAlY bond-coatings with excellent thermal cyclic resistance suitable for use in high-temperature applications. Cyclic oxidative stability was observed to also depend on the underlying metallic alloy substrate.

Keywords: thermal barrier coatings; coating structure; plasma spraying; thermal cycle; high-temperature applications; microstructure studies

1. Introduction

Materials designed to enhance performance and reduce gas emissions in various industrial applications such as aero- and land-based gas turbines and automotive systems are subjected to very high temperatures under harsh environments [1]. The surface modification technique most commonly used to protect these materials against high temperatures and harsh environments is the thermal barrier coating (TBC). A conventional TBC comprises two layers of coatings on the base material. The bond-coat that is directly applied onto the substrate is usually intermetallic MCrAlY [2–6], where M is either Ni, Co, NiCo [3,5,7], or CoNi [2,5,8–10]. The difference in the cases of NiCo and CoNi is the main alloying element: in the first case, Ni is the main alloying element, whereas for the second case Co is the main alloying element. However, CoNiCrAlY intermetallics are most commonly used for industrial TBC applications [9,11]. MCrAlY coatings were observed to be in a two-phase structure comprising the γ-phase (a solid solution of Ni, Co, and Cr), the β-phase (an intermetallic of Ni and Al), and some compositions of tri-nickel aluminide (Ni_3Al) γ'-phase [7].

CoNiCrAlY has the advantage of excellent hot corrosion protection at higher temperatures rather than that of hot corrosion resistance [5]. Most of the studies related to CoNiCrAlY are related to coatings prepared by either cold gas dynamic spraying systems (CGDSs) [2] or high-velocity oxy-fuel (HVOF) [2,8–10,12–14]. In contrast, Richer *at al.* [2] reported that the best quality of deposition of CoNiCrAlY could be achieved by air plasma spraying (APS). Therefore, APS is widely used for bond coating of CoNiCrAlY [15–20] because of its various advantages such as easy deposition of a thick coating, low cost, low power consumption, and a small equipment footprint.

Oxidation tests of the CoNiCrAlY coatings have been conducted to investigate the vulnerability of the coatings at high temperatures. Oxidation tests of a HVOF deposited nanostructured CoNiCrAlY coating at 900°C, 925°C for 72

Corresponding author: Dipak Kumar E-mail: dipakmnnit@gmail.com

h, and 1000°C for durations ranging from 1 to 96 h yielded a duplex oxide scale composed of an inner layer of alumina with an outer layer of Cr_2O_3, $NiAl_2O_4$, or other spinel-structured oxide [8]. The isothermal oxidation tests of CoNiCrAlY coatings prepared using CGDSs, HVOF, and APS techniques at 1000°C for 100 h resulted in predominantly alumina scale in the microstructures of the CGDS coatings and chromia (Cr_2O_3) or dispersed nickel oxide (NiO) in the microstructures of the HVOF coatings. In the case of APS coatings, the samples exhibited greater porosity and oxide content, with substantial amounts of undesirable NiO and mixed spinel-type oxides in the early stages of the oxidation tests [2].

Other factors that have not been investigated in the case of CoNiCrAlY coatings are nonetheless known to affect the adherence of similar top-coats and bond-coats. These factors include the effect of crystal structure, grain size distribution, fineness of the bond-coat powder particles used for coating deposition, and the nature of plasticity of the CoNiCrAlY coating materials.

The objective of the present study was to investigate the microstructural stability of APS-deposited CoNiCrAlY bond coatings on Inconel 800 (IN800) and Hastelloy C-276 superalloy substrates for high-temperature applications before and after thermal cyclic loadings. The objective was to investigate the ability of the bond-coat to protect the underlying metallic alloy substrate in the case of damage to the top-coat.

The phases and microstructure of the as-sprayed CoNiCrAlY conventional coatings produced by APS techniques were characterized by X-ray diffraction (XRD), transmission electron microscopy (TEM), scanning electron microscopy (SEM), field-emission scanning electron microscopy (FESEM), and atomic force microscopy (AFM). The phases and microstructure were also analyzed by XRD, SEM, and FESEM after thermal cyclic testing of the bond-coat to investigate its thermal resistance against cyclic variation of temperature from 1100°C to room temperature.

2. Materials and methods

2.1. Bond-coat fabrications and characterization

Selected substrates IN800 and Hastelloy C-276 were grit-blasted using brown fused alumina particles of abrasive grit size 24 μm at 2.53×10^5 Pa pressure and at a distance of 200 mm to remove surface impurities, increase the surface roughness, and obtain good mechanical interlocking between the coating surface and the substrate surface [21]. The dimension of the substrates was 25 mm × 25 mm × 3 mm. The chemical compositions of the Superni IN800 and Hastelloy C-276 substrates are shown in Tables 1 and 2, respectively. A bond-coat of (150 ± 30) μm thicknesses of Co32Ni21Cr8Al0.5Y powder (chemical composition as per AMDRY 9951, black color, gas-atomized spherical shape, Oerlikon Metco, Wolhen, Switzerland) with a grain size distributed in the range of −38 to +5.5 μm was deposited onto the surface of the substrate. APS was performed using an APS system equipped with an F_4-MB plasma gun (Oerlikon Metco, Wolhen, Switzerland) [22]. Coatings were performed at M/s Sai Surface Coatings and Technology, Patencheru (Hyderabad), India. Coating thickness was measured using digital Vernier calipers and a screw gauge. The optimal APS parameters for deposition of the bond-coat were deduced; the results are reported in Table 3.

Table 1. Chemical composition of IN800 superalloy

wt%

C	Si	Mn	S	P	Cr	Mo	Co	Fe	Ni
0.078	0.39	0.641	0.012	0.021	19.966	0.086	0.036	32.407	Balance

Table 2. Chemical composition of Hastelloy C-276 superalloy

wt%

C	Si	Mn	S	W	Cr	Mo	Co	Fe	Ni
0.007	0.051	0.586	0.004	4.214	15.557	15.127	1.115	6.624	Balance

Table 3. APS spraying process parameters for the CoNiCrAlY bond-coat

Current / A	Voltage / V	Primary gas (Ar) / ($L\cdot min^{-1}$)	Secondary gas (H_2) / ($L\cdot min^{-1}$)	Powder feed rate / ($g\cdot min^{-1}$)	Spray distance / mm	Power / kW
550	67	43	9.5	20	102	37

The samples for microstructural analysis were cut very slowly using a low-speed cutter equipped with a diamond-embedded wafering blade to minimize possible cutting damage to the coating. To achieve a good surface finish, the samples were ground starting with 400-mesh silicon carbide emery paper to 4/0 super-finishing-mesh-quality paper [21]. The samples were characterized by SEM (ZEISS EVO Series model EV015), FESEM (JSM-7100F, JEOL), TEM (JEM 2100, JEOL, Japan), HRTEM (JEM 2100, JEOL, Japan), and AFM (model 5500 scanning probe microscope, Agilent Technologies, USA). Phase analysis was carried out by XRD on a diffractometer (model Smart Lab 3KW, M/s RIGAKU, Japan) equipped with a Cu K_α radiation source (λ = 0.154186 nm) operated at 40 kV and 30 mA. XRD analysis was conducted in the diffraction angle (2θ) range from 20° to 70° at a scanning rate of 0.04°/min. The crystal structure was determined by selected-area electron diffraction (SAED; JEM 2100, JEOL, Japan).

The topography and microstructural evolution images of the bond-coat deposited onto IN800 superalloy and Hastelloy C-276 superalloy were collected using contact-mode AFM (model 5500 scanning probe microscope, Agilent Technologies, USA).

2.2. Thermal cyclic resistance tests

A programmable box-type cycling furnace [23–24] was used for studying the thermal cyclic resistance of the bond-coat. The thermal cyclic tests were performed for 1364 cycles at a highest cycling temperature of 1100°C with a dwell time of 45 min at the maximum temperature. Thereafter, specimens were allowed to cool for 15 min at room temperature by forced convection. The thermal-cyclic-tested bond-coat samples were subsequently analyzed by XRD (model Smart Lab 3KW, M/s RIGAKU, Japan) using Cu K_α radiation (λ = 0.154186 nm) generated at 40 kV and 30 mA and FESEM (JSM-7100F, JEOL).

3. Results and discussion

3.1. Microstructure of the as-sprayed bond-coat

Fig. 1 shows the XRD spectra of the as-sprayed CoNiCrAlY conventional coating. The most intense peak was attributed to the (111) atomic plane of γ-phase-rich Co and was observed at a diffraction angle of 43.7° (JCPDS No. 00-15-0806); the γ′-phase-rich Ni peak, which was also attributed to the (111) plane, was observed as a secondary peak at a diffraction angle of 44.5° (JCPDS No. 00-004-0850). The reflection of the primary peak, which represents the (200) atomic planes of a Ni-rich phase (JCPDS No. 00-041-1057), was observed at a diffraction angle of 42.2°. Peaks attributable to the solid solution of Co–Ni–O (major amount) of the γ/γ′-phase were observed, along with peaks resulting from insignificant amounts of Cr–Al–Y, which was confirmed on the basis of JCPDS Nos. 00-15-0806, 00-004-0850, and 00-041-1057 and on the basis of previously reported results [2,8,10].

Another peak at 44.6° associated with the peak at 43.7° was attributed to β-phase NiAl (JCPDS No. 00-020-0019) [8]. Although low-intensity β-phase peaks are also observed, they are suppressed by the high-intensity peaks of the γ/γ′-phase, indicating the dominance of the latter phase. The XRD results further suggest that an amorphous phase is present in the as-prepared coating, which we attribute to the coating being created by spray atomization, a process known to induce fast particle solidification via high cooling rates. In addition, in the case of very fine particles with smaller diameters, the crystallinity is underdeveloped, resulting in amorphous microstructures.

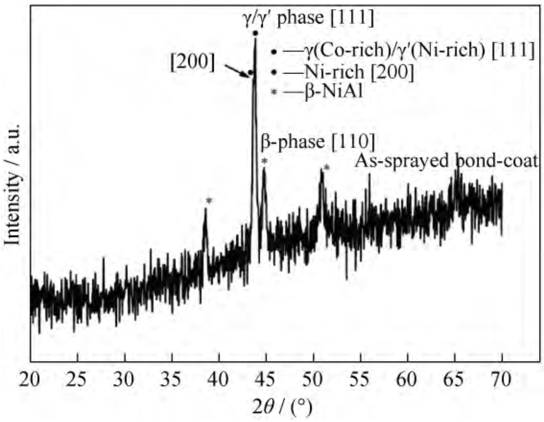

Fig. 1. XRD pattern of as-air plasma sprayed CoNiCrAlY showing γ/γ′ phase.

Fig. 2 presents the SAED pattern of the as-sprayed CoNiCrAlY conventional coating. This diffraction pattern in the form of circular rings suggests that the deposited coatings are polycrystalline and are composed of microsized γ-phase grains. Notably, long-range ordering spots are observed, thus confirming the solid solution (Co–Ni) of the γ/γ′-matrix. The ring-like shape of the diffraction pattern indicates a fine grain size, thereby suggesting the presence of fine precipitates of the β-NiAl phase within the γ/γ′-matrix (Fig. 1). The presence of both the γ- and β-phases in the ring diffraction pattern corroborates the XRD results. On the contrary, the presence of an amorphous microstructure is not observed in the diffraction pattern in Fig. 2. We attribute this lack of an observed amorphous phase to the high-intensity diffraction related to the crystalline structures, which hinders the observation of the amorphous radiance in the diffraction pattern. Fig. 3 shows the lattice spacing of crystal systems, as evaluated through HR-TEM. The *d*-spacing (~0.21 nm) of the γ/γ′-matrix corresponds the (111) atomic planes corresponding to the 2θ diffraction angle of 43.7° in Fig. 1.

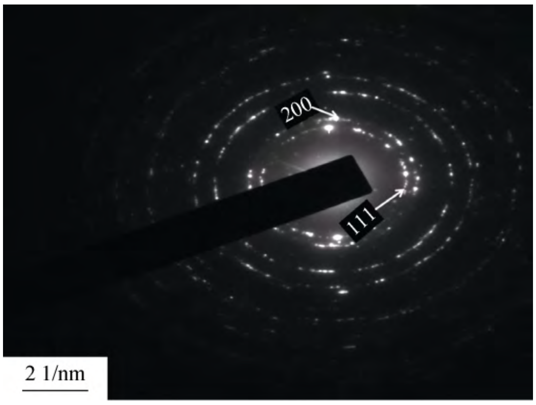

Fig. 2. SAED pattern indexing corresponding to the as-sprayed CoNiCrAlY bond-coat.

The morphology of the as-sprayed CoNiCrAlY conventional coating is shown in Fig. 4(a). The coating exhibits spherical splat morphology and the particle size ranges from 5 to 37 μm. One arrow in Fig. 4(a) denotes melted coating particles with the spherical splat shape; the laminar structure is shown in a circled region. The particle exhibits good plasticity. Fig. 4(b) shows the elemental analysis results for the CoNiCrAlY bond-coat.

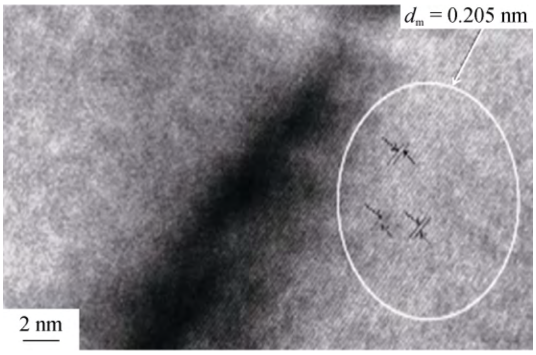

Fig. 3. HR-TEM micrograph of the as-sprayed CoNiCrAlY bond-coat.

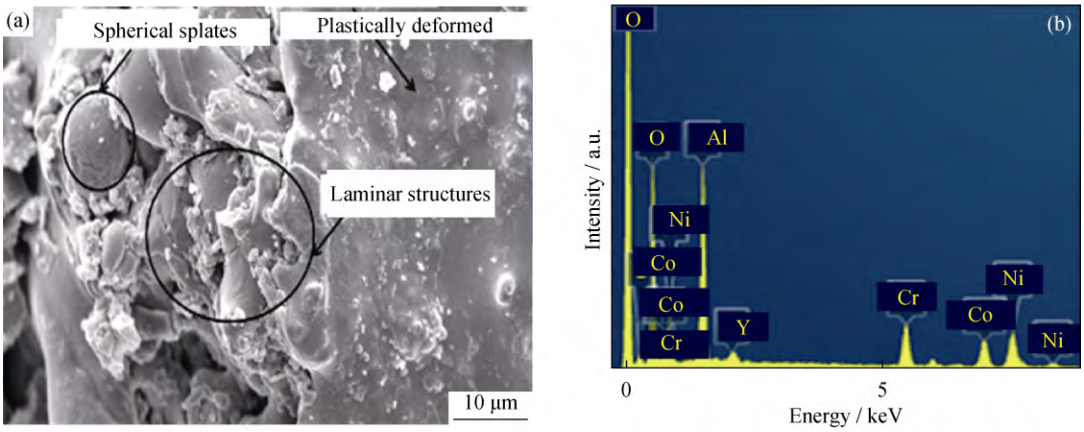

Fig. 4. SEM micrograph (a) and elemental analysis (b) of the as-sprayed CoNiCrAlY bond-coat.

Fig. 5 shows bright-field (BF) TEM images of the as-sprayed CoNiCrAlY conventional bond-coat. The outer coating (the lighter one), as depicted in Fig. 5, is formed mainly by Co, Ni, and O, with minor amounts of Cr, Al, and Y. The inner layer (the darker one) is formed mainly by Cr, Al, and O, with minor amounts of Co, Ni, and Y [2,9]. The thicknesses of both layers appear to be not uniform; the outer layer, in particular, grew very inhomogeneously. The dark layer in Fig. 5 represents the low-intensity β-phase, whereas the light layer represents the high-intensity γ/γ′-phase. It also confirms the presence of very fine-grained precipitates (β-NiAl) embedded in the γ/γ′-matrix. These β-phase precipitates were assumed to have a spherical morphology and grain sizes on the order of nanometers. Observations of the BF image in Fig. 5 further corroborate the XRD results in Fig. 1 and the SAED patterns in Fig. 2.

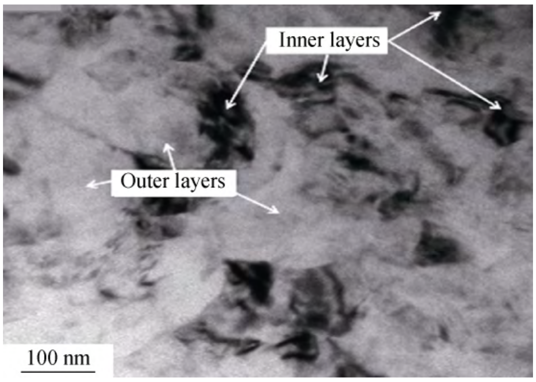

Fig. 5. Bright field TEM image of the as-sprayed bond-coat.

Fig. 6 shows the average grain size distribution of the CoNiCrAlY as-sprayed bond coating; the results in this figure indicate a bimodal distribution, where some of the grains grow to between 20 and 120 nm. This bimodal distribution implies that the nanograins of some of the deposited sprayed particles grow. However, some larger grains in the size range from 100 to 120 nm are also observed. A comparable level of growth of nanograins has also been observed in HVOF bond coatings of CoNiCrAlY [8]. The larger grains are due to partial melting of particles or to particles being subjected to less deformation during deposition of spray particles. A histogram of the grain size was constructed on the basis of AFM images. The best-fitting curve of the average grain size distribution was obtained using the Gaussian equation:

$$y = y_0 + \left(\frac{A}{w \times \sqrt{\left(\mathrm{PI}/2 \right)}} \right) \times \exp\left[-2 \times \left(\frac{x - x_\mathrm{c}}{w^2} \right) \right],$$

where x is the weight function, y is an independent parameter, w is the full-width at half-maximum (FWHM), PI is the principal intensity of grain distribution (in terms of height), and y_0, A, and x_c are constant values.

A scanning electron microscope cannot analyze the pattern of a coating microstructure. We therefore performed AFM analysis. Fig. 7 shows the topography of an as-sprayed CoNiCrAlY conventional bond-coat at various magnifications ranging from the nanometer to the micrometer scale. Figs. 7(a) and 7(b) shows the coating topography in two-dimensional (2-D) and three-dimensional (3-D) images, respectively. The 2-D image (Fig. 7(a)) shows the spherical shape of the coating material in the encircled regions, although grain growth was more clearly observed in the three-dimensional (3-D) image (Fig. 7(b)). Crop-like growth of grains was observed in the 3-D image, which also shows the grain growth of the coating microstructure in the columnar structure, similar to a potato crop. This crop-like structure cannot be observed clearly using SEM [9]. The observed unevenness of the grain explains the non-uniformity of the coating microstructure and the roughness of the coating surface. The growth typically follows an initial stage of heterogeneous nucleation in a columnar pattern.

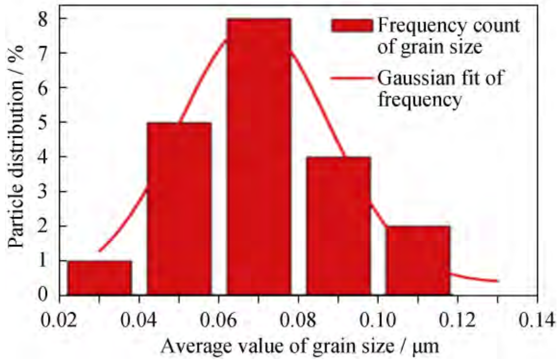

Fig. 6. Histogram of the average grain size of the as-sprayed CoNiCrAlY bond-coat.

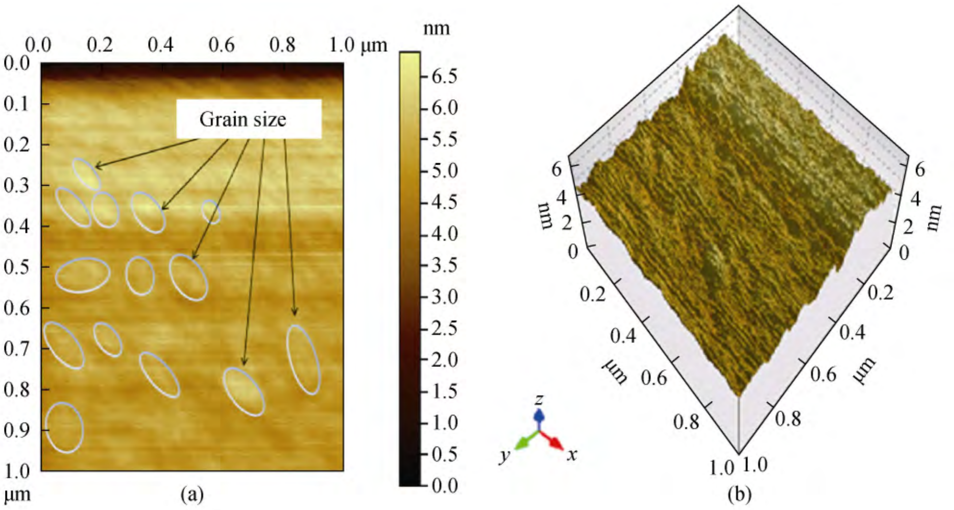

Fig. 7. Topography of the CoNiCrAlY coating at 1 μm^2 scan area: (a) 2-D image; (b) 3-D image.

The plastic deformation and action of heterogeneity of the crystalline closed-packed structure of the bond-coat during deposition of CoNiCrAlY coatings not only provides good adhesion bonding for TBCs but also results in high oxidation, corrosion, erosion, and wear resistance in high-temperature applications. The grain growth of CoNiCrAlY coatings at room temperature is responsible for the stability against oxidation because of the presence of intermetallic elements. The presence of different elements such as Co, Ni, Cr, Al, and Y demonstrate the heterogeneity of the crystal, confirming the close-packed structures, such as face-centered cubic (FCC), hexagonal close-packed (HCP), or body-centered cubic (BCC) structures, of crystalline solids with good thermal resistance.

3.2. Thermal cyclic resistance of the bond-coat

The effects of the bond-coat composition on the thermal cyclic resistance were investigated using an automotive thermal cyclic furnace (M/s Therelek Furnace Pvt. Ltd., Thane, India). The coated specimens were heated at the maximum furnace temperature of 1100°C with a dwell time of 45 min and then forcefully air cooled for 15 min at room temperature. This cycle was repeated for 1364 cycles. A comparative study of the thermal cyclic resistance of the bond-coat on two different superalloys enabled a comparison of the relative adhesion behaviors of the two different metallic substrates and revealed different lifetimes for high-temperature applications. The results of thermal cyclic tests are presented in Fig. 8. The initial increase in mass indicates the formation of an additional layer, which might be a thermally grown oxide (TGO) layer in the form α-alumina (α-phase of Al_2O_3). Alumina layers are known to be resistive to high temperatures. With increasing temperature and time, a mixed oxide layer began to form along with the alumina layer, thus increasing the mass of the substrate. This layer also resists high temperatures. With additional time, this mixed oxide layer might thicken, resulting in a decrease in the adhesiveness of the bond-coat and the onset of mass loss. Fig. 8 presents the lifetime of the bond-coat depending on the selection of substrate and the oxidation behavior in terms of scale growth rates and scale adhesion. The cyclic oxidation tests also show the creep resistance properties of the bond-coat. The slight decrease in mass with increasing number of thermal cycles is mainly due to brittleness of oxide layer formed on the bond-coat, but this oxide layer loses bonding strength with time.

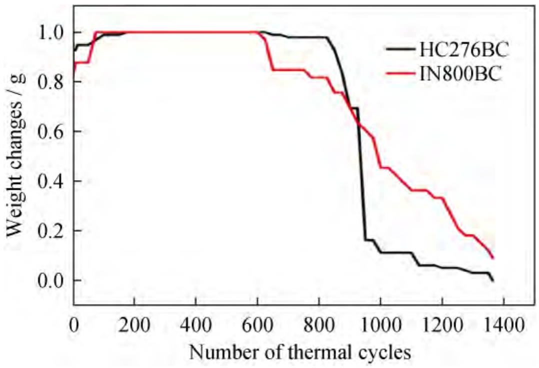

Fig. 8. Weight changes of the bond-coat with number of thermal cycles.

Furnace thermal cyclic tests of bond-coated specimens of IN800 superalloy and Hastelloy C-276 superalloy substrates showed different types of direction patterns, as is evident in the XRD patterns in Fig. 9. These XRD patterns show that both materials are composed of a tetragonal phase but with different atomic orientations. Some monoclinic phases were also detected, as per JCPDS PDF No. 020-0777. The tetragonal structure matches JCPDS PDF No. 021-0008 and JCPDS PDF No. 020-0776, with Ni–Al compositional oxide formation of $NiAl_2O_4$ in the bond-coated IN800 [25]. Notably, the low-intensity peaks of the monoclinic phase are suppressed by the high-intensity peaks of the tetragonal phase. This result is attributed to the high thermal stability of the CoNiCrAlY bond-coat composition. In addition, a match with JCPDS PDF No. 021-008 provides evidence for the presence of intermetallic compounds such as NiAl and tri-nickel aluminide (Ni_3Al) in the Hastelloy C-276 bond-coat.

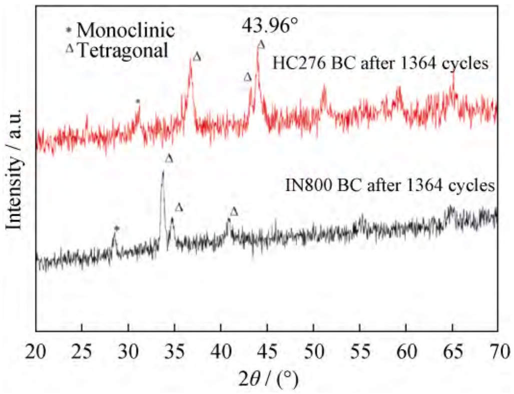

Fig. 9. XRD spectrum of bond-coat CoNiCrAlY on two different superalloys.

The thermal stability of the bond-coats was also characterized at very high resolution by FESEM. We collected high-resolution FESEM images to check the thermal resistance of the bond-coats against fracture or oxidation. Fig. 10(a) shows the oxidation behavior of the bond-coat deposited onto IN800. It shows considerable deformation of the bond-coat materials as a result of high thermal stresses under thermal cyclic loading. The presence of deformable bond-coat materials results in creep oxidation in the form of an intermetallic layer. Fig. 10(b) shows a backscattered electron image of the IN800 bond-coat. An image of the blackish-grey coating are presented in Fig. 10(b). The blackish and grey regions indicate the $NiAl_2O_4$ intermetallic compound, as confirmed by the energy-dispersive X-ray spectroscopy (EDS) analysis results in Fig. 10(c). FESEM micrographs of the bond-coat on Hastelloy C-276 after thermal cycling are shown in Fig. 11. The creep behavior of the bond-coat composition is observed in Fig. 11(a), whereas Fig. 11(b) shows the backscattered image of the bond coated Hastelloy C-276 superalloy substrate. The EDS analysis results in Fig. 11(c) show that the nature of the bond-coat on

Hastelloy C-276 differs from that of the bond-coat on the IN800 superalloy substrate. A feature common to both superalloy bond-coats was the presence of an alumina layer. Over time, the nature of the bond-coat deposited onto the different superalloys changed. In the case of the Hastelloy C-276 bond-coat, Cr_2O_3 formed before a mixed oxide compound.

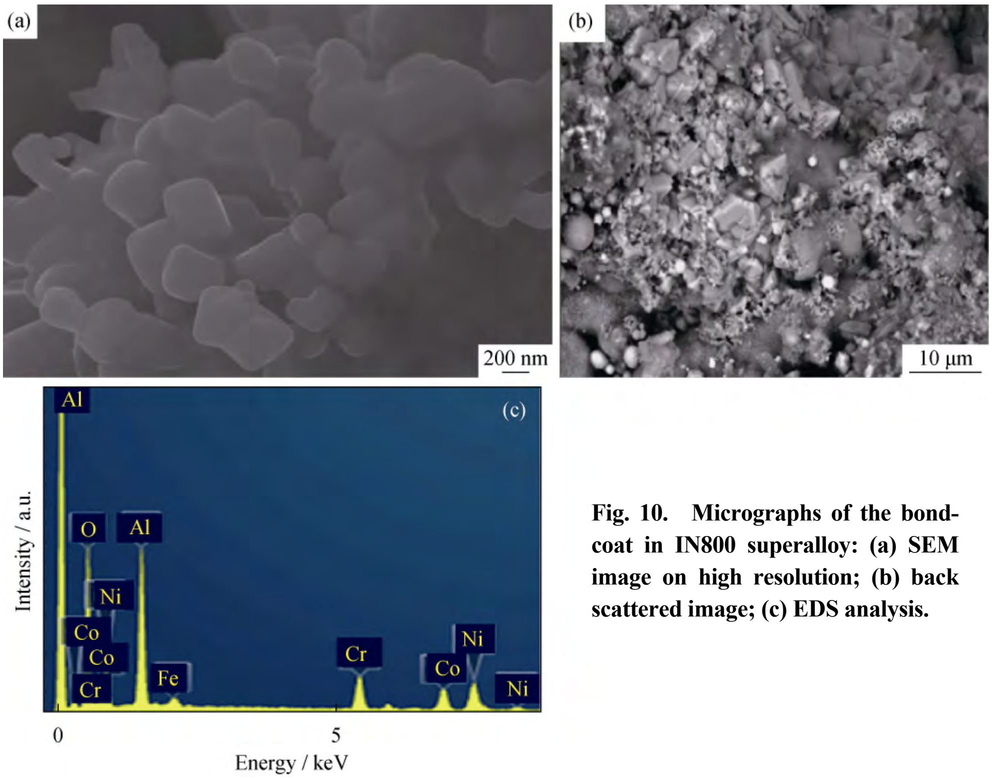

Fig. 10. Micrographs of the bond-coat in IN800 superalloy: (a) SEM image on high resolution; (b) back scattered image; (c) EDS analysis.

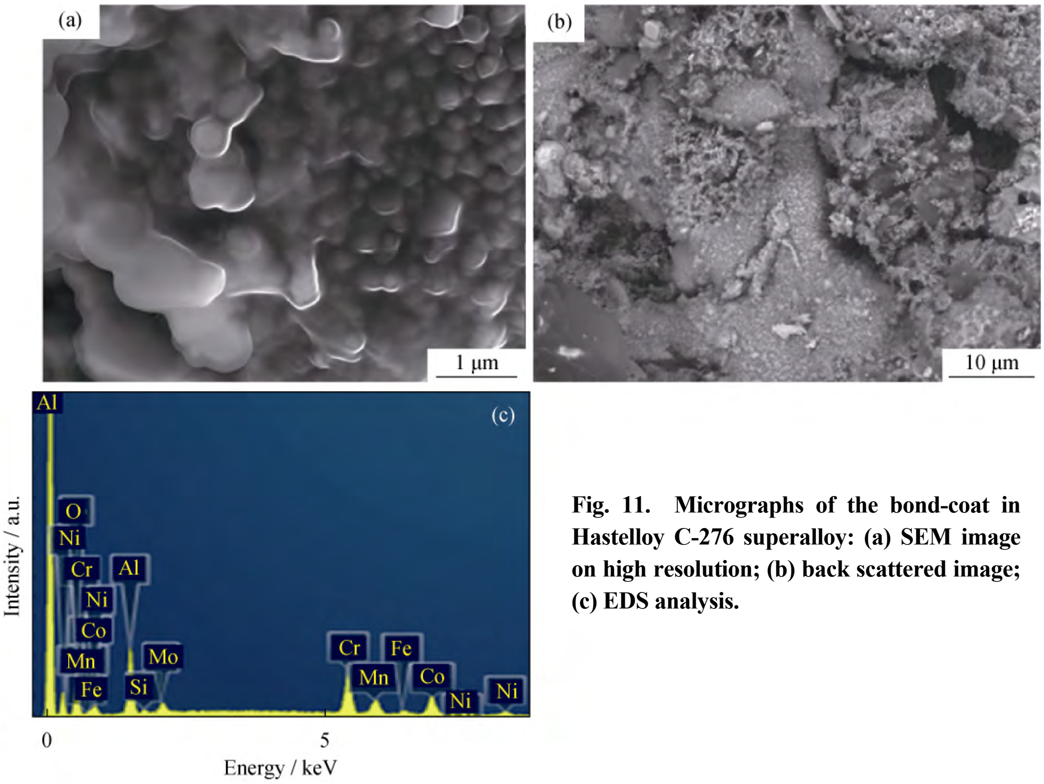

Fig. 11. Micrographs of the bond-coat in Hastelloy C-276 superalloy: (a) SEM image on high resolution; (b) back scattered image; (c) EDS analysis.

The EDS analysis results in Fig. 10(c) indicate that Co participated in the growth of the thermally grown oxide layer (i.e., α-alumina growth). We also observed that the main contributions of ordering-I elements decrease in the order Al > Ni > Co > Cr in the thermally grown oxide layer on the Superni IN800 bond-coat, whereas the contributions of ordering-II elements decrease in the order Al > Ni > Cr > Co in the thermally grown oxide layer on the Hastelloy C-276 bond-coat. Ordering-II elements are observed to be more beneficial than ordering-I elements, as evident from the high thermal cyclic stability of their oxide layers. Ordering-II delays the formation of the mixed oxide over the thermally grown oxide (TGO) layer. This delay of the mixed oxide formation in the Hastelloy C-276 bond-coat provides a greater thermal stability in comparison to the stability of bond-coated Superni IN800 (Fig. 8). Mixed oxides are known to be brittle by nature and become a source of crack formation, causing early coating damage. The selection of a substrate is important for achieving good thermal stability of the bond-coat. The thermal stability of the Hastelloy C-276 bond-coat was observed to be greater than that of the Superni IN800 bond-coat. In both the cases, Ni-Al mixed oxide formation was observed to be responsible for the thermal cyclic oxidation resistance (Fig. 10(c) and Fig. 11(c)).

On the basis of the microstructure analysis results, we conclude that the thermal cyclic resistance can be improved by controlling the bond-coat composition, selecting an appropriate substrate, or both.

4. Conclusions

Our results are summarized as follows:

(1) XRD and TEM results demonstrated the relationship between microstructural changes and the deposition process of CoNiCrAlY coatings. High-intensity peaks associated with the γ/γ′-phase and breakup of the spray particles as β-phase precipitates were observed by XRD.

(2) A phase transformation of the microstructure of the deposited material from γ-phase to β-phase was attributed to concentrated plastic deformation resulting from high-velocity impact between spray particles and the metallic alloy substrate during plasma spray deposition.

(3) Grain growth of the coating microstructure of the as-sprayed CoNiCrAlY conventional coating was observed through AFM.

(4) The SEM, TEM, HR-TEM, and AFM results were in close agreement with respect to the phase and microstructure of the CoNiCrAlY conventional coatings at room temperature.

(5) The microstructure of the CoNiCrAlY coatings subjected to thermal cyclic loading confirmed good adhesion bonding, which is beneficial for top-coats subjected to high-temperature cyclic loading.

(6) High cyclic oxidative stability of the CoNiCrAlY coating materials was also observed for protecting the underlying metallic alloy substrate, confirming the suitability of this coating material for TBC applications.

(7) The cyclic oxidative stability of CoNiCrAlY coatings was observed to depend on the underlying metallic alloy substrate.

(8) Elemental analyses confirmed that a Ni–Al mixed oxide is mainly responsible for the stability against oxidation during high-temperature cycling.

Acknowledgements

The authors acknowledge the testing facilities of XRD and SEM provided by the Center for Interdisciplinary Research (CIR), Motilal Nehru National Institute of Technology, Allahabad. The financial support provided by Technical Education Quality Improvement Programme-II (TEQIP-II) at MNNIT Allahabad is also gratefully acknowledged.

References

[1] S. Bose, *High Temperature Coatings*, Elsevier Butterworth-Heinemann, Amsterdam, 2007.

[2] P. Richer, M. Yandouzi, L. Beauvais, and B. Jodoin, Oxidation behaviour of CoNiCrAlY bond coats produced by plasma, HVOF and cold gas dynamic spraying, *Surf. Coat. Technol.*, 204(2010), No. 24, p. 3962.

[3] Y. Li, C.J. Li, G.J. Yang, and L.K. Xing, Thermal fatigue behavior of thermal barrier coatings with the MCrAlY bond coats by cold spraying and low-pressure plasma spraying, *Surf. Coat. Technol.*, 205(2010), No. 7, p. 2225.

[4] S.M. Jiang, C.Z. Xu, H.Q. Li, J. Ma, J. Gong, and C. Sun, High temperature corrosion behaviour of a gradient NiCoCrAlYSi coating I: Microstructure evolution, *Corros. Sci.*, 52(2010), No. 5 , p. 1746.

[5] D.R.G. Achar, R. Munoz-Arroyo, L. Singheiser, and W.J. Quadakkers, Modelling of phase equilibria in MCrAlY coating systems, *Surf. Coat. Technol.*, 187(2004), No. 2-3, p. 272.

[6] Y. Gao, M.C. Chen, and C.X. Shi, Study on EB-PVD zirconia thermal barrier coatings for gas turbine blade protection, *Mater. Manuf. Processes*, 14(1999), No. 5, p. 691.

[7] J. Buršík, P. Brož, and J. Popovič, Microstructure and phase equilibria in Ni–Al–Cr–Co alloys, *Intermetallics*, 14(2006), No. 10-11, p. 1257.

[8] D. Mercier, C. Kaplin, G. Goodall, G. Kim, and M. Brochu, Parameters influencing the oxidation behavior of cryomilled CoNiCrAlY, *Surf. Coat. Technol.*, 205(2010), No. 7, p. 2546.

[9] F. Tang, L. Ajdelsztajn, and J.M. Schoenung, Influence of cryomilling on the morphology and composition of the oxide scales formed on HVOF CoNiCrAlY coatings, *Oxid. Met.*, 61(2004), No. 314, p. 219.

[10] F. Tang, L. Ajdelsztajn, G.E. Kim, V. Provenzano, and J.M. Schoenung, Effects of surface oxidation during HVOF processing on the primary stage oxidation of a CoNiCrAlY coating, *Surf. Coat. Technol.*, 185(2004), No. 2-3, p. 228.

[11] A.C. Karaoglanli, A. Turk, I. Ozdemir, and F. Ustel, Comparison of oxidation and thermal shock performance of thermal barrier coatings, *Mater. Manuf. Processes*, 30(2015), No. 6, p. 717.

[12] S. Saeidi, K.T. Voisey, and D.G. McCartney, The effect of heat treatment on the oxidation behavior of HVOF and VPS CoNiCrAlY coatings, *J. Therm. Spray Technol.*, 18(2009), No. 2, p. 209.

[13] W.J. Chen, Degradation of a TBC with HVOF-CoNiCrAlY bond coat, *J. Therm. Spray Technol.*, 23(2014), No. 5, p. 876.

[14] M. Okada, R. Vassen, M. Karger, D. Sebold, D. Mack, M.O. Jarligo, and F. Bozza, Deposition and oxidation of oxide-dispersed CoNiCrAlY bond coats, *J. Therm. Spray Technol.*, 23(2014), No. 1-2, p. 147.

[15] W.S. Rathod, A.S. Khanna, R.C. Rathod, and S.G. Sapate, Wear and corrosion behavior of CoNiCrAlY bond coats, *J. Inst. Eng. India Ser. C*, 95(2014), No. 3, p. 261.

[16] G.X. Wang, R. Goswami, S. Sampath, and V. Prasad, Understanding the heat transfer and solidification of plasma-sprayed yttria-partially stabilized zirconia coatings, *Mater. Manuf. Processes*, 19(2004), No. 2, p. 259.

[17] R.C. Novak, A.P. Matarese, R.P. Huston, A.J. Scharman, and T.M. Yonushonis, Development of thick thermal barrier coatings for diesel applications, *Mater. Manuf. Processes*, 7(1992), No. 1, p. 15.

[18] L. Wang, Y. Wang, X.G. Sun, J.Q. He, Z.Y. Pan, and C.H. Wang, Thermal shock behavior of 8YSZ and double-ceramic-layer $La_2Zr_2O_7$/8YSZ thermal barrier coatings fabricated by atmospheric plasma spraying, *Ceram. Int.*, 38(2012), No. 5, p. 3595.

[19] H. Jamali, R. Mozafarinia, R.S. Razavi, and R. Ahmadi-Pidani, Comparison of thermal shock resistances of plasma-sprayed nanostructured and conventional yttria stabilized zirconia thermal barrier coatings, *Ceram. Int.*, 38(2012), No. 8, p. 6705.

[20] W.R. Chen, X. Wu, and D. Dudzinski, Influence of thermal cycle frequency on the TGO growth and cracking behaviors of an APS-TBC, *J. Therm. Spray Technol.*, 21(2012), No. 6, p. 1294.

[21] D. Kumar, K.N. Pandey, and D.K. Das, Characterization of air plasma based 7YSZ aluminum alloys thermal barrier systems for hot zone, *Proc. Inst. Mech. Eng. Part L J. Mater. Des. Appl.*, doi: 10.1177/1464420716640570.

[22] D. Kumar and K.N. Pandey, Optimization of the process parameters in generic thermal barrier coatings using the Taguchi method and grey relational analysis, *Proc. Inst. Mech. Eng. Part L J. Mater. Des. Appl.*, doi: 10.1177/1464420715602727.

[23] D. Kumar and K.N. Pandey, Study on thermal fatigue behavior of plasma sprayed yttria-zirconia thermal barrier coatings (TBCs) systems on aluminum alloy, *Int. J Mech. Prod. Eng.*, 2(2014), No. 3, p. 19.

[24] D. Kumar, K.N. Pandey, and D.K. Das, Thermal cyclic resistance behavior of Inconel 800 super alloy substrate with thermal barrier coatings by plasma spraying, *Mater. Today Proc.*, 2(2015), No. 4-5, p. 3156.

[25] Q.Z. Cui, S.M. Seo, Y.S. Yoo, Z. Lu, S.W. Myoung, Y.G. Jung, and U. Paik, Thermal durability of thermal barrier coatings with bond coat composition in cyclic thermal exposure, *Surf. Coat. Technol.*, 284(2015), p. 69.